

1 **Critical Evaluation of Strong Ground Motions in Izmir and Implications for Future Earthquake Simulation**

2 **Results**

3 Sahin Caglar Tuna

4 Ass. Prof. Dr.; Yasar University, Izmir

5 **ABSTRACT**

6 Izmir, a major city in western Turkey, is located in a highly seismic region, subject to frequent earthquakes due to
7 its proximity to active fault systems. This paper critically evaluates the strong ground motions recorded in Izmir,
8 with a focus on understanding the implications for urban infrastructure and future seismic hazard mitigation.
9 Historically available data is collected and compared with the available ground motion prediction equations
10 (GMPE). Later, the most appropriate prediction equation is selected and used to determine the target response
11 spectrum. 2020 Sisam earthquake is a well-documented seismic event and the data from the stations are then used
12 to further calibrate the 1D site response model. Lastly, possible future events are generated and results are
13 compared with the current Turkish Earthquake Code (TEC). Amplification factors prescribed by code for İzmir
14 Bay have been surpassed by projected future events, highlighting the necessity for reassessment. Therefore, region-
15 specific seismic zoning should be established when standard code practices fall short in accounting for significant
16 site effects. Concrete recommendations about local site modification factors and evaluations on this topic have
17 been provided within the article.

18 **Keywords:** Ground motion prediction equations, Site response, Future events, Local site modification factors

19

20

21

22

23

24

25

26

27

28

29

30

31

32 **1. INTRODUCTION**

33 Throughout history, İzmir—Turkey’s third-largest city—has been repeatedly affected by destructive earthquakes
34 due to its location near active fault systems along the Aegean coast. With its dense urban fabric and economic
35 significance, understanding seismic hazard in the region is crucial for enhancing urban resilience and risk
36 mitigation. The city is underlain by thick Quaternary alluvial deposits, which are known to significantly amplify
37 incoming seismic waves, especially in deep basin areas. This amplification poses a serious threat to the built
38 environment, particularly for buildings with fundamental periods resonating with the local site response.

39 The 2020 Samos earthquake provided a striking demonstration of these effects: in districts such as Bayraklı, field
40 observations and numerical simulations showed that spectral accelerations in the 0.7–1.0 s period range exceeded
41 Turkish Earthquake Code (TEC, 2018) predictions by factors of 4 to 6 (Cetin et al., 2022; Gülerce et al., 2022).
42 These unexpected amplifications have been attributed to complex basin geometries, soft soil layers, and high
43 impedance contrasts (Cetin et al., 2023). Such site-specific effects, which are not fully captured in conventional
44 design spectra, highlight the urgent need for detailed ground motion characterization in İzmir

45 Although numerous studies have addressed local site effects or assessed GMPEs independently, most fall short of
46 providing an integrated framework that unites strong-motion recordings, deterministic scenario modeling, and
47 code-based spectrum comparison. This gap underscores the need for regionally calibrated GMPEs and basin-aware
48 design spectra that can explicitly account for spatially variable amplification across İzmir Bay. Conventional site
49 classification approaches, moreover, often fail to capture the spatial variability in seismic demand across basin
50 environments like İzmir Bay.

51 This study bridges that gap by combining nearly three decades (1996–2024) of empirical strong-motion data with
52 residual-based GMPE evaluations and site-specific response analyses using a validated DeepSoil model. By
53 incorporating these elements into a unified simulation framework, the study highlights how code-based design
54 spectra—when lacking localized amplification considerations—may significantly underestimate seismic demand
55 in urban basins. The proposed methodology thus offers a regionally calibrated and practically transferable
56 foundation for performance-based seismic design in İzmir and similar tectonic settings.

57 The purpose of this study is divided into two main parts: First part is to evaluate the strong ground motions recorded
58 in Izmir during past seismic events, particularly focusing on their effects on local geotechnical conditions and built
59 environments. In the second part, a future earthquake scenario and potential engineering outcomes will be
60 examined by using the findings obtained in the first part.

61 To achieve these goals, the study follows a structured methodology comprising the following steps:

- 62 a. Data Collection: Gathering historical earthquake data from the Izmir region, including earthquake
63 magnitudes, source-to-site distances, and PGA measurements.
- 64 b. Selection of GMPEs: Choosing GMPE models that are applicable to the regional tectonic and geological
65 conditions.

- 66 c. Comparison of GMPE Predictions and evaluation of GMPE Accuracy: Comparing the predicted PGA
67 values from different GMPEs with the observed values from historical earthquakes. Differences were
68 observed between the predicted and actual ground motions, emphasizing the importance of site-specific
69 adjustments in GMPEs for accurate seismic hazard assessment. Using statistical methods, such as Root
70 Mean Square Error (RMSE), to assess the accuracy of the GMPE predictions and identify the most
71 reliable model for the Izmir region. Apply necessary improvements for the prediction equations to comply
72 with the specific directivity and near fault effects.
- 73 d. 1D site response analysis were firstly validated with the available recordings and then set up for the future
74 earthquake scenarios.
- 75 e. Developing target spectra using the outcomes of 3rd step, evaluating future earthquakes in the region and
76 comparison with the current TEC results.
- 77 f. The study concludes with recommendations on refining seismic hazard models to account for local site
78 effects and improving the predictive accuracy of GMPEs in areas with complex soil profiles. These
79 findings have implications for earthquake-resistant design and site-specific seismic risk mitigation
80 strategies.

81 By integrating a comprehensive set of strong-motion recordings, residual-based GMPE evaluation, and site-
82 specific response analysis within a deterministic simulation framework, this study establishes a regionally
83 calibrated seismic design basis for İzmir. The methodology not only captures basin-induced amplification
84 effects often overlooked by code-based spectra but also provides a transferable approach for seismic hazard
85 assessment in other urban basins with similar geological and tectonic settings.

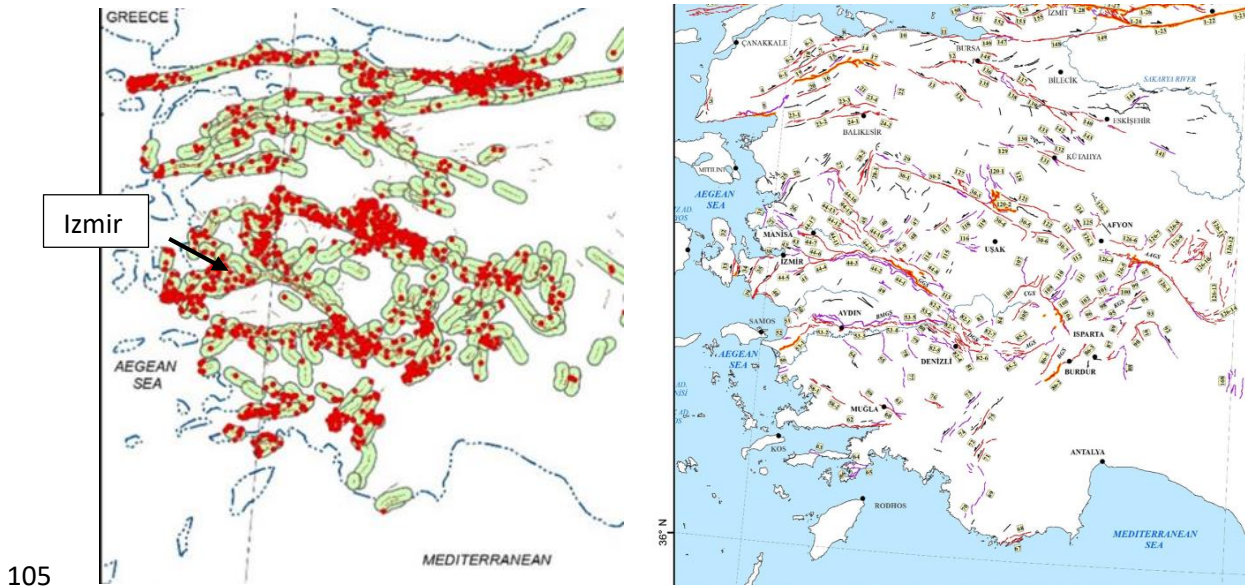
86 1.1. Regional Seismicity and Geological Settings of Izmir Bay

87 İzmir is located in the western part of Turkey, within the tectonically active Aegean Extensional Province. This
88 region is characterized by widespread normal faulting, primarily driven by back-arc extension associated with the
89 subduction of the African Plate beneath the Eurasian Plate along the Hellenic Trench (McKenzie, 1978).
90 Historically, the region has experienced several destructive earthquakes, most notably the 1688 and 1778 events,
91 which caused widespread structural damage and loss of life in the İzmir area (Tepe et al., 2021). The ongoing
92 crustal extension has resulted in crustal thinning, frequent shallow-focus earthquakes, and persistent seismicity
93 throughout Western Anatolia (Emre et al., 2005).

94 The seismotectonic framework of the region includes a complex network of both normal and strike-slip faults.
95 These structures, many of which are segmented and capable of multi-segment ruptures, are comprehensively
96 documented in the GIS-based Active Fault Database of Turkey (Emre et al., 2018). This database provides detailed
97 information on fault activity classifications, geometries, and slip rates essential for seismic hazard assessments.
98 The İzmir metropolitan area lies in close proximity to several active fault zones, as illustrated in Figure 1,
99 underscoring the city's exposure to significant seismogenic sources.

100 In addition to this tectonic complexity, the İzmir Bay region is underlain by thick accumulations of Quaternary
101 alluvial and sedimentary deposits. These geologic conditions contribute to pronounced site-specific amplification

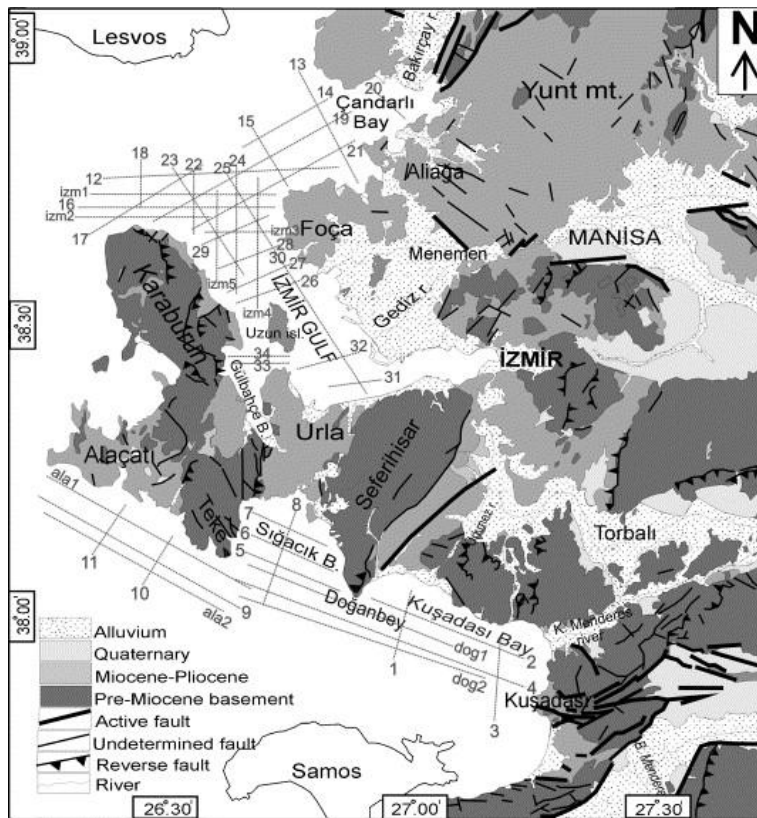
102 effects, especially in soft soil basins where seismic waves may be significantly intensified. Consequently, the
103 combined influence of active faulting and local geology necessitates detailed ground motion characterization and
104 site response analysis for reliable seismic risk assessment (Ocakoglu et al., 2005; Akyol et al., 2006).



105
106 Figure 1. Active Seismic Faults and recent earthquakes in the region (Emre et.al, 2018)

107 The geological framework of İzmir is markedly heterogeneous, comprising a combination of sedimentary basins,
108 alluvial plains, and sporadic rock outcrops. These spatially variable ground conditions play a pivotal role in
109 modulating seismic wave propagation, particularly through amplification mechanisms driven by soft soil layers
110 and impedance contrasts. This phenomenon is especially pronounced in areas where unconsolidated sediments
111 dominate the subsurface, resulting in significant variations in shaking intensity and spectral content during
112 earthquakes.

113 A regional geological map illustrating the distribution of major lithological units and active fault lines is presented
114 in Figure 2. The map clearly delineates the extent of alluvial plains and the underlying bedrock zones, offering
115 critical insight into potential site response variations across the study area.



116

117 Figure 2. Geology map of the study area and location of the seismic fault lines (Adapted from Ocakoglu et.al,
118 2005).

119 The İzmir Bay region includes several structurally controlled sedimentary basins such as the Gediz Graben and
120 margins of the Menderes Massif. These basins are filled with geologically young, unconsolidated sediments that
121 are highly susceptible to seismic wave amplification. Much of the coastal zone, particularly surrounding the bay,
122 is composed of loose alluvial deposits with low stiffness and high porosity. These characteristics are known to
123 significantly enhance ground motion amplitudes and contribute to localized damage concentration during seismic
124 events.

125 **2. Compilation of the strong motion dataset and predictive performance of current ground motion**
126 **models**

127 Ground Motion Prediction Equations (GMPEs) are empirical or semi-empirical formulations developed to estimate
128 expected ground motion parameters—such as peak ground acceleration (PGA)—at a given site, based on variables
129 including earthquake magnitude, source-to-site distance, and local site conditions (Gülerce et al., 2022). These
130 models are fundamental tools in probabilistic seismic hazard analysis (PSHA) and performance-based earthquake
131 engineering.

132 Given the seismically active nature of the Western Anatolian region and the complex geological and tectonic
133 characteristics of İzmir, selecting a regionally appropriate and predictively reliable GMPE is critical. Various
134 models have been proposed for different tectonic environments; for instance, the Euro-Mediterranean region is

135 well-represented by the NGA-Europe models developed by Akkar and Bommer (2010) and Akkar et al. (2014).
136 In Turkey, Kalkan and Gülkan (2004) introduced a site-dependent GMPE based on national datasets. However,
137 many of these models exhibit limitations, including restricted magnitude–distance ranges, insufficient treatment
138 of site-specific effects, or limited representation of near-fault ground motions.

139 In this study, eight GMPEs from the NGA-West1 and NGA-West2 projects were selected due to their
140 methodological robustness, comprehensive magnitude–distance coverage, and well-established site adjustment
141 formulations based on V_{s30} . Models such as Boore et al. (2014) and Chiou and Youngs (2014) were included,
142 owing to their wide adoption in international hazard frameworks and their applicability to site-specific studies in
143 urban basins like İzmir.

144 To evaluate their predictive performance, a strong-motion dataset comprising 33 earthquake records from 1996 to
145 2024 was compiled from the Turkish Disaster and Emergency Management Presidency (AFAD). These events
146 span a broad spectrum of moment magnitudes (M_w) and source-to-site distances, thus enabling a robust assessment
147 of model performance across varying seismic scenarios (Table 1).

148 All records were obtained from two well-instrumented stations located in the Bornova district: Station 3502 (V_{s30}
149 = 270 m/s) and Station 3522 (V_{s30} = 249 m/s), both corresponding to NEHRP Site Class D (FEMA, 2001)
150 conditions. The use of two stations with similar geotechnical classifications helps minimize variability from local
151 soil conditions and enhances the comparability of model outputs, making the findings particularly relevant to the
152 soft-soil conditions prevalent in much of urban İzmir.

153 Despite the regional relevance and methodological consistency of the selected GMPEs, several epistemic
154 uncertainties persist. These stem from potential regional discrepancies in model calibration, simplified rupture-to-
155 site distance metrics, and the scarcity of near-fault recordings within the compiled historical dataset. Moreover,
156 although both recording stations are categorized as NEHRP Site Class D (FEMA, 2001), subtle variations in
157 subsurface stratigraphy and nonlinear site response characteristics may not be fully captured through V_{s30} -based
158 adjustments alone. These limitations highlight the need for ongoing regional calibration efforts and the integration
159 of high-resolution geotechnical and seismic data to improve ground motion modeling accuracy in complex urban
160 basins such as İzmir.

161 The predicted peak ground acceleration (PGA) values from each GMPE were then compared with the observed
162 PGA values from the 33 historical records. The comparison results are summarized in Figure 3, while Table 2
163 provides a list of the selected GMPEs.

164

165

166

167

168 Table 1.Important characteristics of the historical seismic events

Event No	Event Name	Mw	Epicentral Distance - km	Fault Mechanism	Event Depth -km	PGA Max - cm/s2
1	2.04.1996	4.9	71.81	Normal	12	18.42
2	14.11.1997 Aegean Sea (Kusadası)	5.8	128.79	Normal	12	6.03
3	09.07.1998 Aegean Sea	5	75.48	Normal	12.5	27.06
4	22.01.1999 Buca-İzmir	3.4	9.95	Strike Slip	5	2.985
5	17.08.1999 Golcuk (İzmit)	7.6	346.5	Strike Slip	15.9	10.8
6	21.01.2002 Turgutlu (Manisa)	4.8	60.11	Normal	11.7	6.981
7	10.04.2003 - Seferihisar	5.7	37.45	Strike Slip	18.7	78.57
8	17.04.2003 Seferihisar (İzmir)	5.2	61.55	Strike Slip	11.5	8.851
9	29.01.2005	4.9	47.67	Normal	20	6.131
10	17.10.2005 - Urla	5.8	58.21	Strike Slip	11	13.12
11	17.10.2005 - Urla	5.4	56.17	Strike Slip	20.5	16.51
12	20.10.2005 - Urla	5.9	58.98	Strike Slip	15.4	31.773
13	24.12.2005 Akhisar (Manisa)	4.9	64.85	Normal	6	3.14
14	19.05.2011 Simav (Kutahya)	5.7	180.7	Normal	24.46	5.533
15	8.01.2013 - Aegean Sea	6.2	194		26.83	3.642
16	24.05.2014 - Aegean Sea	6.5	255.78		25	7.659
17	19.07.2014 - Konak- İzmir	3.7	10	Strike Slip	6.98	9.47
18	02.06.2017 Ayvacik (Canakkale)	5.3	154.13	Normal	14.16	1.466
19	12.06.2017-Karaburun	6.2	43.87	Normal	15.86	58.306
20	12.06.2017-Karaburun	6.2	89.62	Normal	15.86	25.499
21	17.06.2017 Aegean Sea	5.3	81.15	Normal	9.11	9.42
22	20.07.2017 Aegean Sea(Bodrum)	6.5	169.93	Normal	19.44	4.44
23	08.08.2019 Bozkurt (Denizli)	6	218.49	Normal	10.92	0.39
24	18.02.2020 Kırkağaç (Manisa)	5.2	91.02	Normal	6.98	4.662
25	26.06.2020- Saruhanlı-Manisa	5.5	64.1	Normal	9.29	7.109
26	28.06.2020 Ege Denizi (Mugla)	5.2	214.57	Normal	61.42	3.375
27	30.10.2020 Sisam	5.1	72.95	Normal	7.71	7.056
28	30.10.2020- Sisam	7	75.57	Normal	16.54	73.72
29	21.04.2021-Sehzadeler-Manisa	4.9	40.19	Normal	13.2	9.673
30	21.06.2021 Aegean Sea (Datca)	5.3	228.34	Normal	14.74	0.61
31	11.04.2022- Buca - İzmir	4.9	9.81	Strike Slip	14.47	48.59
32	01.10.2023 Lesvos	5	130.95	Normal	14.95	1.708
33	27.01.2024 Aegean Sea (Kusadası)	5.1	52.46	Normal	8.51	7.632

169

170 Table 2. GMPEs Used In this Study

No	Ground Motion Prediction Equation
1	AS08: Abrahamson & Silva (2008) NGA Model
2	BA08: Boore & Atkinson (2008) NGA Model
3	CB08: Campbell & Bozorgnia (2008) NGA Model
4	CY08: Chiou & Youngs (2008) NGA Model
5	ASK14: Abrahamson, Silva & Kamai (2014) NGA-West2 Model
6	BSSA14: Boore, Stewart, Seyhan & Atkinson (2014) NGA-West2 Model
7	CB14: Campbell & Bozorgnia (2014) NGA-West2 Model
8	CY14: Chiou & Youngs (2014) NGA-West2 Model

171

172

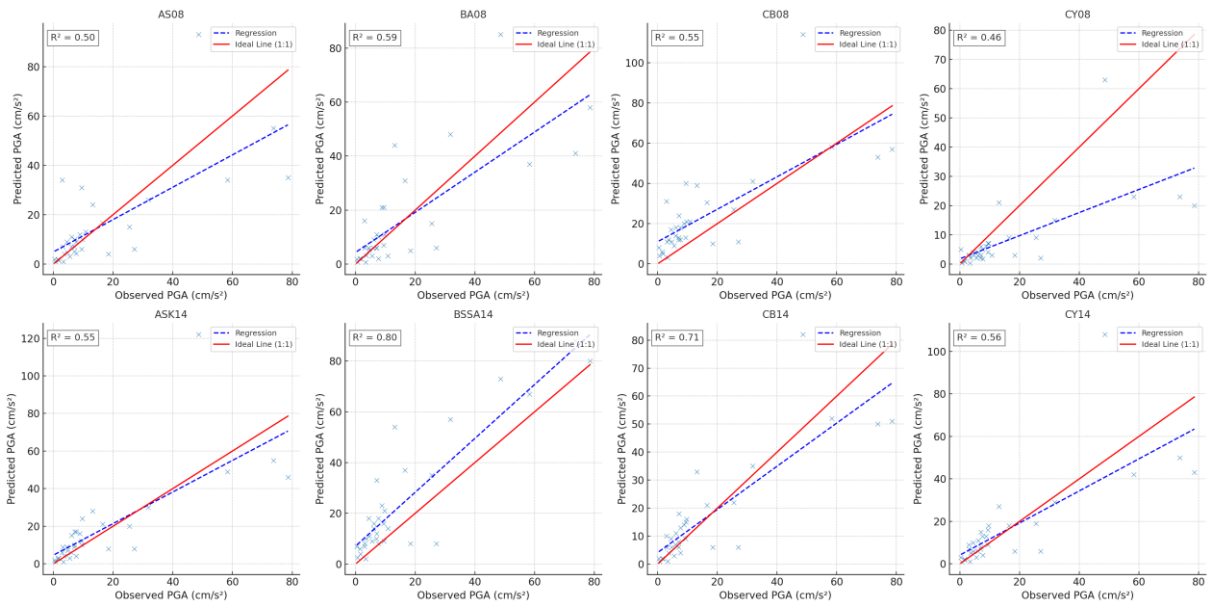
173 To quantify the predictive accuracy of the selected GMPEs, statistical error analyses were conducted using two
 174 commonly employed metrics: the Root Mean Square Error (RMSE) and the Coefficient of Determination (R^2).
 175 These metrics aim to assess which GMPE most accurately captures the observed peak ground accelerations (PGA)
 176 across a range of earthquake magnitudes and site conditions. The comparative results are presented in Table 3.

177 RMSE is widely used to evaluate the deviation between observed and predicted values. It is particularly sensitive
 178 to large errors, thereby emphasizing models that perform consistently across the dataset. The RMSE is defined as:

$$179 \text{RMSE} = \sqrt{\frac{1}{N} \sum_{i=1}^N (PGA_{\text{observed},i} - PGA_{\text{predicted},i})^2} \quad (1)$$

180 Where:

- 181 - N is the number of the earthquake records
- 182 - i is the index of each event,
- 183 - $PGA_{\text{observed},i}$ is the observed PGA for the i -th earthquake
- 184 - $PGA_{\text{predicted},i}$ is the predicted PGA for the i -th earthquake based on the GMPE.



185
 186 **Figure 3.** Scatter plots comparing observed and predicted PGA values for eight GMPEs. (The 1:1 line (red)
 187 represents perfect prediction, while the regression line (blue, dashed) and R^2 values indicate model-specific fit
 188 quality.)

189 To interpret the predictive capacity of each GMPE, scatter plots comparing observed versus predicted PGA values
 190 were generated for all eight models (Figure 3). The 1:1 reference line denotes perfect prediction, while deviations
 191 from this line indicate systematic bias or dispersion. A variety of factors contribute to discrepancies among the
 192 models, including site-specific amplification effects, differences in magnitude–distance scaling, depth
 193 parameterization, and the internal constants adopted by each model.

194 Since isolating these effects is not feasible with the available dataset, the analysis relies on statistical performance
 195 metrics—specifically R^2 and RMSE—to rank the models. Based on these results (Table 3), CB14 and BSSA14
 196 emerged as the most accurate and consistent predictors, demonstrating the highest R^2 (0.71 and 0.80, respectively)
 197 and lowest RMSE values (11.03 and 13.39 cm/s^2 , respectively).

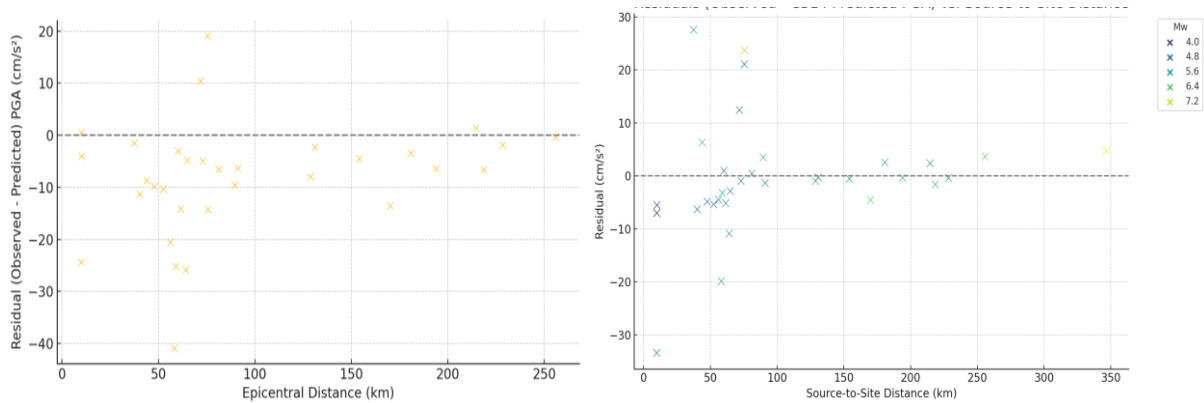
198 Table 3. Result of GMPE Error Analysis

GMPE	R^2	RMSE (cm/s^2)
AS08	0.5	14.85
BA08	0.59	13.53
CB08	0.55	17.11
CY08	0.46	16.75
ASK14	0.55	16.08
BSSA14	0.8	13.39
CB14	0.71	11.03
CY14	0.56	14.61

199
 200 Although GMPEs provide spectral acceleration predictions across multiple periods, their most reliable and
 201 discriminative predictions typically occur at very short periods, where model-to-model variability is smallest and
 202 empirical constraints are strongest. For this reason, many regional GMPE screening studies rely on PGA or other
 203 short-period intensity measures as the primary basis for model selection (e.g., Boore et al., 2014; Chiou & Youngs,
 204 2014; Kalkan & Gülkan, 2004; Karaca et al., 2021; Huang et al., 2023). Consistent with this practice, the current
 205 study evaluates GMPE performance using PGA—which is directly recorded, least affected by processing
 206 assumptions, and strongly correlated with $Sa(T)$ at short periods ($T \leq 0.2$ s). In subsequent analyses (Section 4),
 207 GMPEs are not used to generate full response spectra; instead, they provide the short-period amplitude anchor on
 208 rock, while the long-period spectral characteristics are controlled by near-fault directivity effects and site-specific
 209 nonlinear amplification validated using the 2020 Samos earthquake. Thus, the use of PGA for GMPE screening is
 210 methodologically consistent with the intended application of the GMPEs in Section 4.

211 To better understand model-specific behavior, residual analyses were conducted for CB14 and BSSA14. Although
 212 both models performed well in terms of overall fit, they exhibited distinct systematic biases. CB14 tended to
 213 underpredict observed PGA, especially for short-distance and high-magnitude events. This behavior may be
 214 attributed to near-fault effects and local site amplification not fully accounted for in the model's global calibration.
 215 In contrast, BSSA14 showed a tendency to overpredict ground motions, particularly for low-magnitude and far-
 216 field events, suggesting that the model is conservative under low-shaking conditions. These trends are clearly
 217 illustrated in the residual plots in Figure 4a and 4b, where CB14 residuals are color-coded by magnitude.

218 These contrasting residual patterns underscore the limitations of applying globally calibrated GMPEs to complex
 219 local conditions without adjustment. Rather than indicating model inadequacy, they highlight the necessity for
 220 regionally validated ground motion models—especially in geologically heterogeneous urban basins like İzmir.
 221 These findings support a growing consensus in the literature advocating for localized GMPE calibration as a
 222 critical step toward improved seismic hazard assessment.



223
 224 **Figure 4.** Residual plots for the two top-performing GMPEs: (a) BSSA14 – residuals vs distance (b) CB14 –
 225 residuals vs distance with magnitude color-coding.

226 **3. Site response validation analysis for future predicted events**

227 To simulate the site-specific seismic response for potential future scenarios, a validated one-dimensional (1D) Site
 228 Response Analysis (SRA) framework was adopted. The validation was performed using strong-motion recordings
 229 from the well-documented 2020 Samos (Sisam) Earthquake, which provided a rare and valuable opportunity to
 230 calibrate the numerical models under actual seismic loading conditions.

231 The earthquake occurred on October 30, 2020, with a moment magnitude of Mw 6.9, and an epicenter located
 232 approximately 14 km northeast of Samos Island in the Aegean Sea. Although the rupture occurred offshore, the
 233 event produced significant structural damage in İzmir due to its shallow focal depth, rupture directivity effects,
 234 and strong site amplification within the alluvial basin. Numerous strong-motion stations across İzmir recorded the
 235 event (Figure 5), including stations situated on soft alluvial soils and others positioned on rock outcrops. This
 236 diversity enabled a robust comparative evaluation of site effects (Kwok et al., 2007; Kramer, 1996).

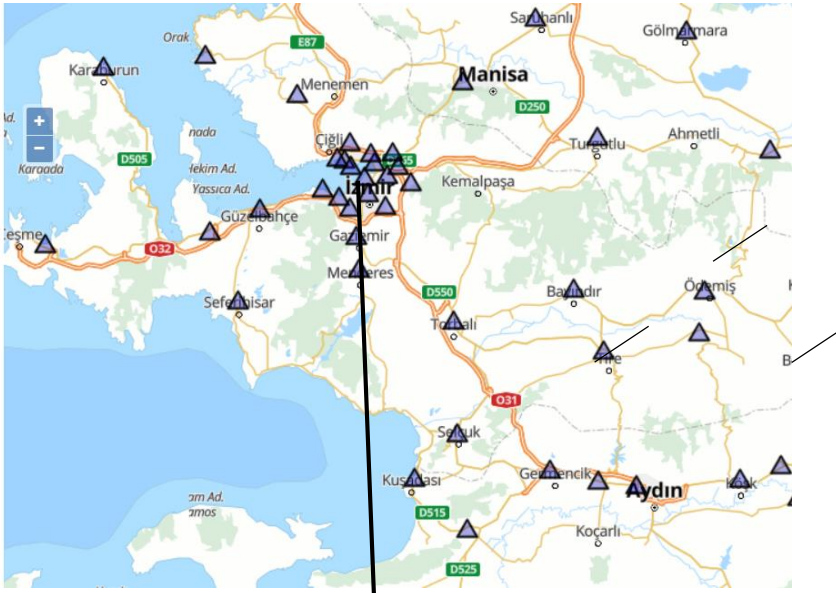
237 The 1D SRA simulations were conducted by propagating the 3514 rock-outcrop motion—obtained from the AFAD
 238 strong-motion network—through the calibrated soil columns at the selected sites. Station 3514, characterized by a
 239 V_{S30} value of 836 m/s, is the only rock site in the study area and therefore provides an appropriate outcrop reference
 240 motion for validation purposes.

241 Four representative locations were selected to capture the geotechnical and geological variability across İzmir:

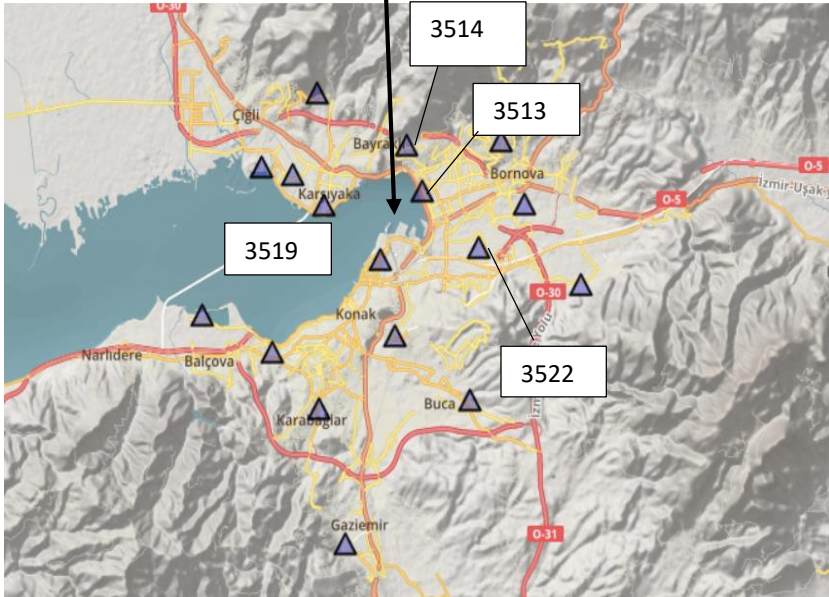
- 242 • Karşıyaka (3519) – basin edge, thick alluvial deposits
- 243 • Bayraklı (3513) – deep soft soils with high amplification potential
- 244 • Bornova (3522) – moderately deep alluvial layers
- 245 • Konak (central district) – urban area with transitional soil conditions

246 These stations collectively reflect the diversity of soil conditions and shaking characteristics across İzmir, enabling
 247 the development of a calibrated and reliable SRA model for subsequent scenario-based simulations.

248



249



250 **Figure 5.** Overview of Stations in Izmir

251 The reference rock station was identified as Station 3514, located near the basin edge, and classified as a rock site
252 based on its $V_{S30} = 836$ m/s. The corresponding PGA values and geotechnical characteristics of all selected stations
253 are presented in Table 4, while their geophysical profiles are illustrated in Figure 6.

254 By comparing observed ground motions with the site response simulations, the model's ability to reproduce
255 frequency-dependent amplification patterns was evaluated. This validation step was critical to ensuring that the
256 calibrated SRA models could be confidently applied to the simulation of future earthquake scenarios, particularly
257 in geologically complex and amplification-prone zones of İzmir.

258

259

260 Table.4 Selected Soil/Rock Sites

Site Name	Region	Vs30 (m/sec)	TEC Site Class	Coordinates	PGA (g)
3514	Bayrakli	836.00	ZB	38.4762 27.1581	0.057 (E-W)
3513	Bayrakli	195.00	ZD	38.4584 27.1671	0.108 (N-S)
3519	Karsiyaka	131.00	ZE	38.4525 27.1112	0.153 (N-S)
3522	Bornova	249.00	ZD	38.4357 27.1987	0.075(E-W)

261 3.1. Soil Characterization and Nonlinear Site Response Modeling

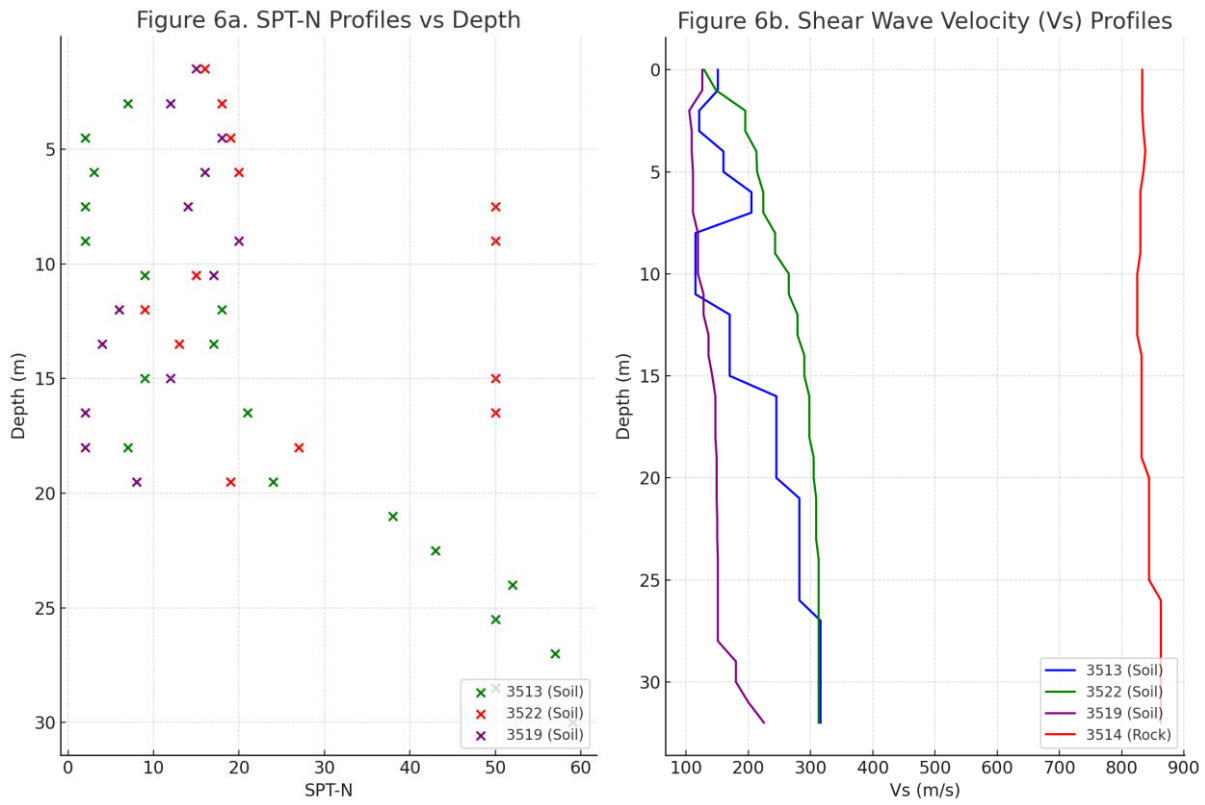
262 Based on borehole logs, standard penetration test (SPT) profiles, and laboratory-based soil classification data, the
 263 upper 20 m of all three soil stations (3513, 3519, and 3522) predominantly consist of soft to medium-stiff fine-
 264 grained soils. These strata are interbedded and transitional in nature, comprising alternating sequences of low-
 265 plasticity clays (CL), high-plasticity clays (CH), and silty sands (SM). With increasing depth, the subsurface
 266 transitions into sandy clays (SC) and dense silty layers, which are characteristic of alluvial depositional
 267 environments. The soil profiles used in the analyses were compiled from deep geotechnical and geophysical
 268 investigations conducted at each station.

269 One-dimensional (1D) site response analyses were conducted using the DeepSoil software (Hashash et al., 2020),
 270 which allows for simulation of nonlinear soil behavior under vertically propagating shear waves. DeepSoil enables
 271 the incorporation of site-specific parameters, nonlinear modulus reduction and damping relationships, and realistic
 272 boundary conditions. The software has been widely applied in recent nonlinear site response studies (e.g., Cetin et
 273 al., 2022), and its reliability is further supported by experimental studies emphasizing the importance of modeling
 274 strain-dependent behavior (Tsai & Liu, 2017; Tsai & Li, 2024).

275 Modulus reduction (G/G_{max}) and damping ratio (D) curves were assigned based on soil classification. The Seed
 276 and Idriss (1970) model was used for cohesionless soils, while the Vucetic and Dobry (1991) curves were adopted
 277 for cohesive soils. The importance of accurate damping formulation was also emphasized by Zalachoris and Rathje
 278 (2015), who demonstrated through borehole array studies that nonlinear behavior and frequency-dependent
 279 damping are critical for reliable site response predictions across different strain levels.

280 Figure 6 presents SPT-N and shear-wave velocity (V_s) profiles for all soil sites and for the reference rock site
 281 (3514). The soil sites reflect soft alluvial conditions, whereas Station 3514—characterized by a V_{s30} of 836 m/s
 282 and classified as NEHRP Site Class B—served as the reference rock motion for all SRA simulations. To accurately
 283 represent the deep basin geometry and ensure correct application of the input motion at the engineering bedrock
 284 level, each soil column was extended to its full geophysical depth. Based on regional MASW, microtremor, and

285 deep-borehole investigations, the total sediment thicknesses were defined as approximately 120 m for Station
286 3513, 250 m for Station 3519, and 90 m for Station 3522



287

288 Figure 6. (a) SPT-N profiles vs. depth and (b) shear wave velocity (V_s) profiles for soil stations (3513, 3519, 3522)
289 and reference rock station (3514).

290 3.2. Validation Results Using the 2020 Samos Earthquake

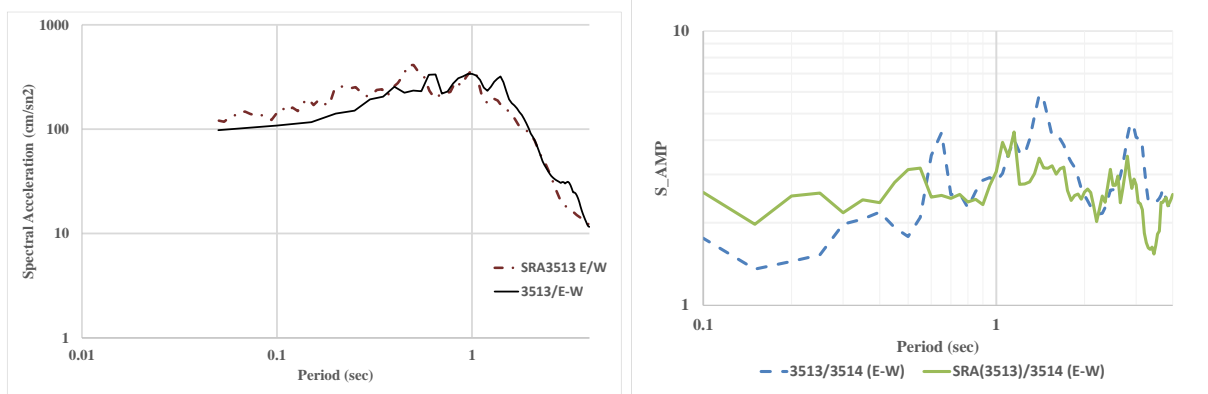
291 Site response analysis results were evaluated for three key locations across İzmir—Karşıyaka (3519), Bayraklı–
292 Bornova (3522), and Konak–Alsancak (3513)—representing varying soil and geophysical conditions within the
293 alluvial basin. The selection of multiple sites enabled assessment of spatial variability and the derivation of a
294 generalized response spectrum that better reflects urban-scale ground motion behavior. Validation was conducted
295 using the 2020 Samos Earthquake recordings, and the comparisons are illustrated in Figures 7 through 9.

296 In each case, spectral response functions derived from SRA were compared with observed site motions. The
297 amplification function $S_{amp} = SR(\text{site}) / SR(\text{outcrop})$ was computed to evaluate frequency-dependent
298 amplification. The station at Konak (3513) showed the most pronounced amplification, with peaks reaching 4.0–
299 4.5 times the input motion at periods around 1.5 seconds. The Bornova station (3522) exhibited similar
300 amplification characteristics, with peak values around 3.0–3.5 in the same period range. These stations share
301 similar geotechnical conditions and are located within the central alluvial basin, which likely contributed to the
302 consistent amplification behavior. In contrast, Karşıyaka station (3519) displayed notable amplification at longer
303 periods, peaking near 2.5 seconds, suggesting differences in basin edge geometry and deeper soil layering effects.

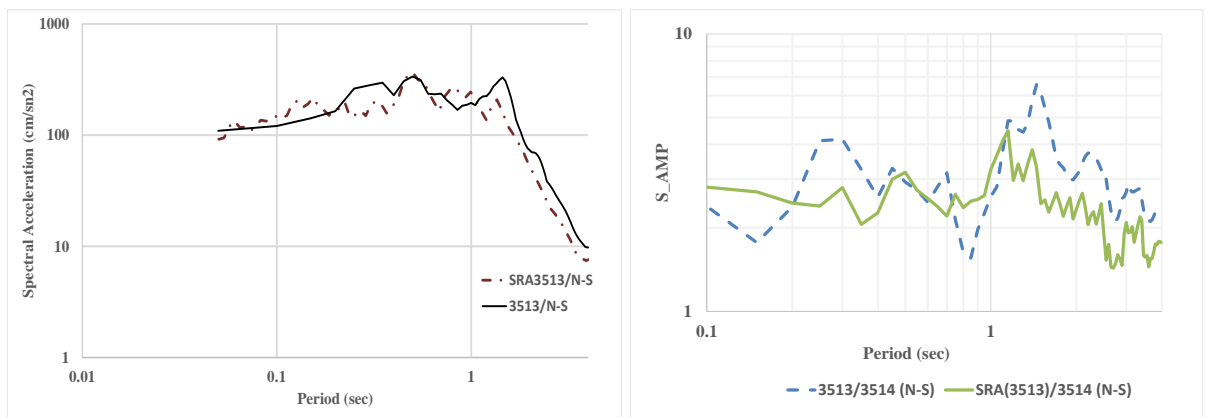
304 These results illustrate the spatial heterogeneity of seismic site response within İzmir and highlight the limitations
305 of using uniform design spectra across geologically diverse urban areas.

306

307

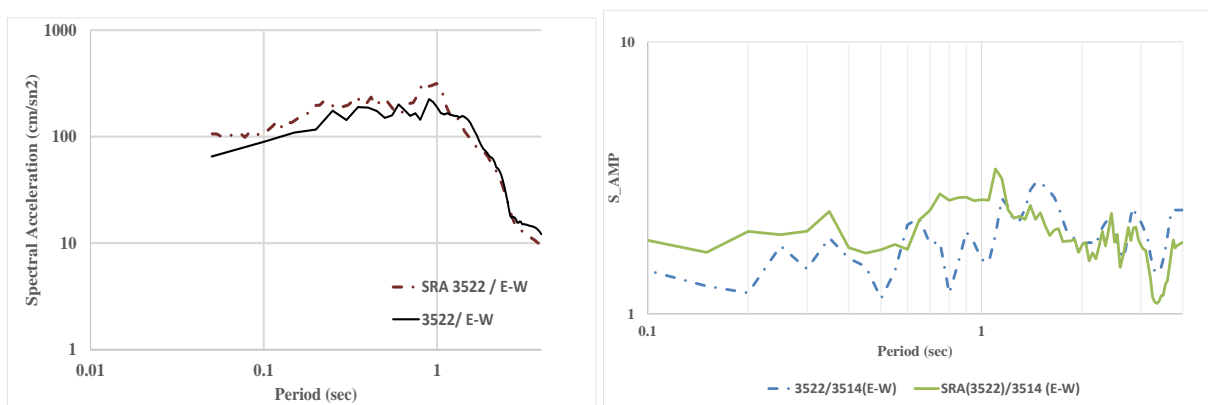


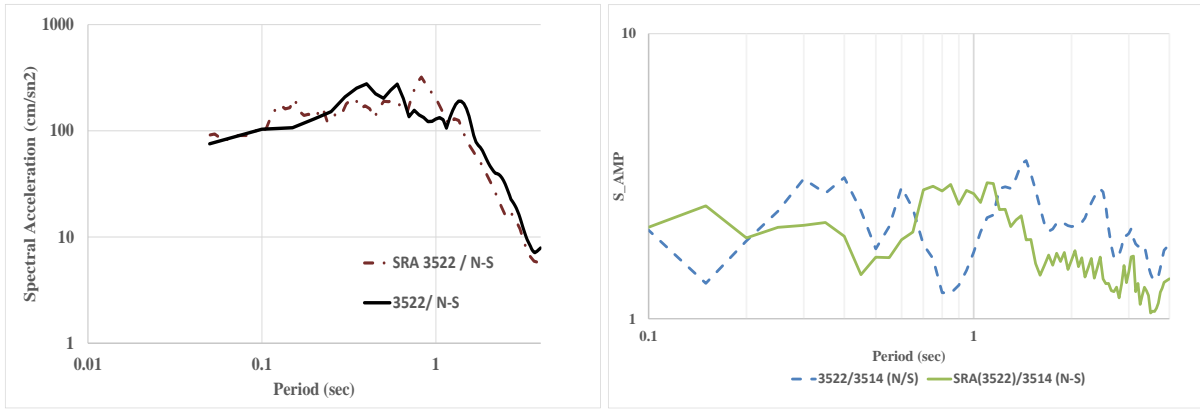
308



309 Figure 7. The comparison of recorded and estimated (SRA) elastic response and amplification spectra for 2020
310 Samos event@station 3513

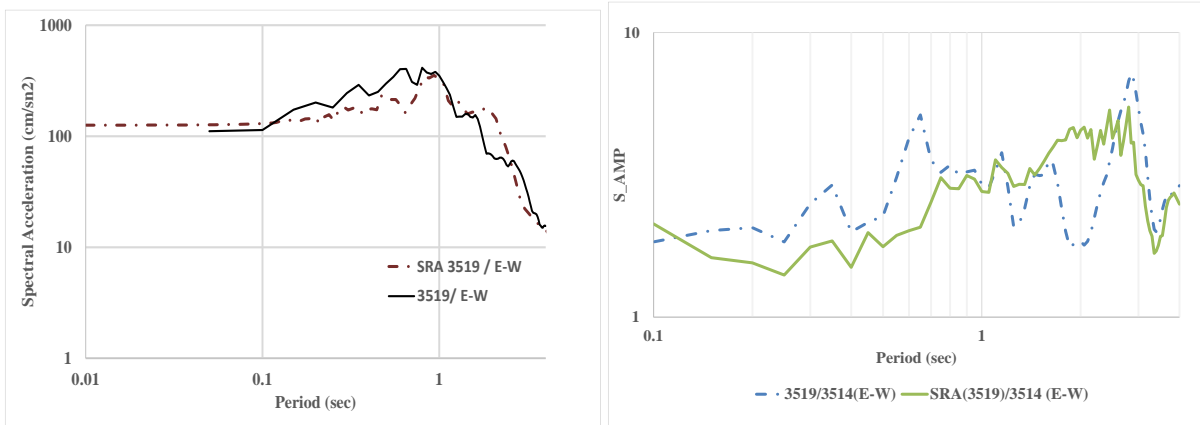
311



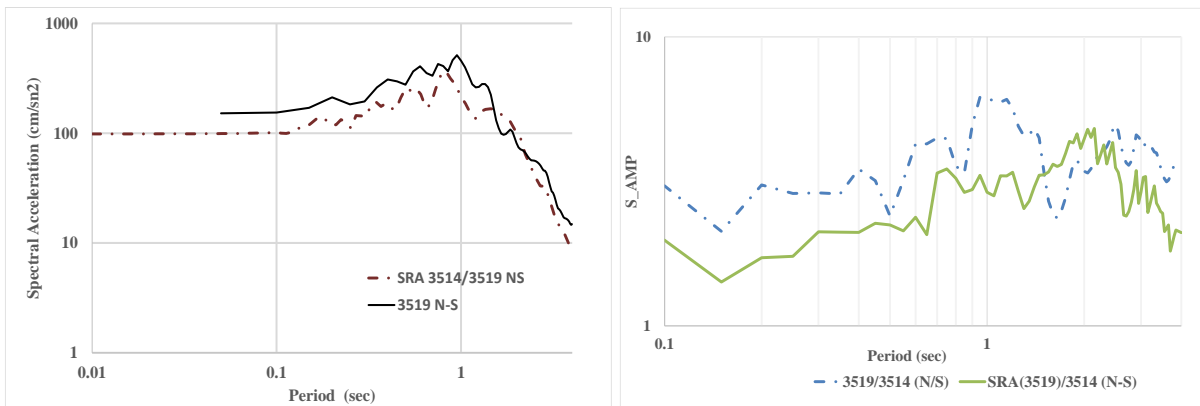


312

313 Figure 8. The comparison of recorded and estimated (SRA) elastic response and amplification spectra for 2020
 314 Samos event@station 3522



315



316

317 Figure 9. The comparison of recorded and estimated (SRA) elastic response and amplification spectra for 2020
 318 Samos event@station 3519

319 The comparison between recorded and simulated acceleration response spectra demonstrates a strong agreement,
 320 particularly within the period range of 0.5–1.5 seconds. This interval corresponds to the fundamental periods of
 321 typical 6- to 10-story reinforced concrete (RC) buildings, which constitute a substantial portion of İzmir's existing

322 building stock. Therefore, amplification in this period range is of particular concern, as it directly increases seismic
323 demand on mid-rise structures.

324 To quantitatively assess the accuracy of the site response simulations, the computed acceleration response spectra
325 were compared with the corresponding recorded ground motion data at six different components (3513e-w, 3513n-
326 s, 3522e-w, 3522n-s, 3519e-w, and 3519n-s). In addition to visual comparisons (see Figure 9), four quantitative
327 metrics were employed to evaluate the degree of agreement between simulated and recorded spectra:

- 328 • Root Mean Square Error (RMSE) – measuring the average deviation,
- 329 • Coefficient of Determination (R^2) – indicating the proportion of variance explained,
- 330 • Goodness-of-Fit Index (GOF) – assessing relative error,
- 331 • Nash–Sutcliffe Efficiency (NSE) – evaluating predictive performance.

332 The computed values for each component are summarized in Table 5.

333 **Table 5.** Validation metrics between recorded and simulated acceleration response spectra.

Component	RMSE (cm/s ²)	R ²	GOF	NSE
3513 E-W	49.36	0.797	0.881	0.797
3513 N-S	51.52	0.759	0.841	0.759
3522 E-W	53.82	0.481	0.831	0.481
3522 N-S	47.64	0.594	0.819	0.594
3519 E-W	60.5	0.73	0.841	0.73

334 As shown in Table 5, RMSE values ranged from 47.6 to 60.5 cm/s², reflecting moderate absolute deviations across
335 components. R^2 values exceeded 0.73 in most cases, except for 3522 E–W, which exhibited lower correlation (R^2
336 = 0.481), likely due to localized variability in soil conditions or measurement noise. The GOF index remained
337 consistently high (>0.81), and NSE values confirmed strong predictive agreement for most components.

338 In particular, the 3513 E–W and 3519 E–W components yielded the best fit, with $R^2 > 0.73$, $GOF > 0.84$, and NSE
339 values supporting excellent agreement. These findings confirm the robustness of the nonlinear SRA model in
340 capturing both the amplitude and spectral shape of the recorded ground motions, especially in soft soil zones with
341 known amplification potential. On average, the 75th percentile of the observed spectra falls within the simulated
342 spectral range, indicating reliable envelope matching across the mid-period band. Similar validation patterns were
343 also reported by Cetin et al. (2024), supporting the consistency of the modeling framework employed in this study.

344 Based on these results, the adopted 1D site response framework is considered both reliable and transferable for
345 future ground motion simulations. Combined with previously validated GMPE selection, this analysis provides a
346 sound basis for generating site-specific target spectra and evaluating regional seismic demand scenarios. The next
347 step involves defining target design spectra for scenario earthquakes and conducting corresponding SRA
348 simulations across selected locations.

349

350 4. Selecting Target Response Spectrum And Evaluating The Results Of Future Events

351 In developing the target response spectrum for the deterministic Mw 6.5 scenario, the median predictions of the
352 selected GMPEs (CB14 and BSSA14) were used primarily to anchor the short-period spectral amplitudes at the
353 reference rock level. This is a common practice in regional seismic hazard studies, where PGA and very short-
354 period S_a values provide a stable and well-constrained baseline. The longer-period portion of the spectrum,
355 however, was shaped by additional physical considerations—including rupture directivity, basin effects, and the
356 nonlinear site response characteristics validated in Section 3—rather than being taken directly from GMPE spectral
357 shapes. This hybrid approach allows the target spectrum to remain consistent with both regional tectonic
358 constraints and locally observed amplification patterns. Based on this framework, ground-motion parameters for
359 the Mw 6.5 event were estimated in alignment with the RADIUS (1997) source definition for the İzmir Fault,
360 whose magnitude potential is further supported by recent models such as EFSM20 and ESHM20.

361 Although the RADIUS model predates more recent fault datasets, its validity is corroborated by contemporary
362 source characterizations such as EFSM20 (Basili et al., 2024), which classifies the İzmir Fault among the active
363 structures with an estimated moment magnitude potential of Mw 6.5–6.7. Additionally, recurrence rate maps from
364 ESHM20 (Danciu et al., 2024) indicate that the İzmir Basin exhibits annual exceedance rates on the order of \log_{10}
365 ≈ -6.5 to -7.0 for events exceeding Mw 6.5. These combined findings support the plausibility and engineering
366 relevance of the selected scenario.

367 A critical factor in site-specific seismic hazard assessment is the near-fault rupture directivity effect, which can
368 significantly amplify long-period ground motions. As originally proposed by Somerville et al. (1997), directivity-
369 induced ground motions occur when seismic energy is focused along the rupture propagation direction, resulting
370 in pulse-like waveforms with high amplitude and short duration. Such effects are particularly significant at sites
371 located within approximately 10–15 km of the rupture plane.

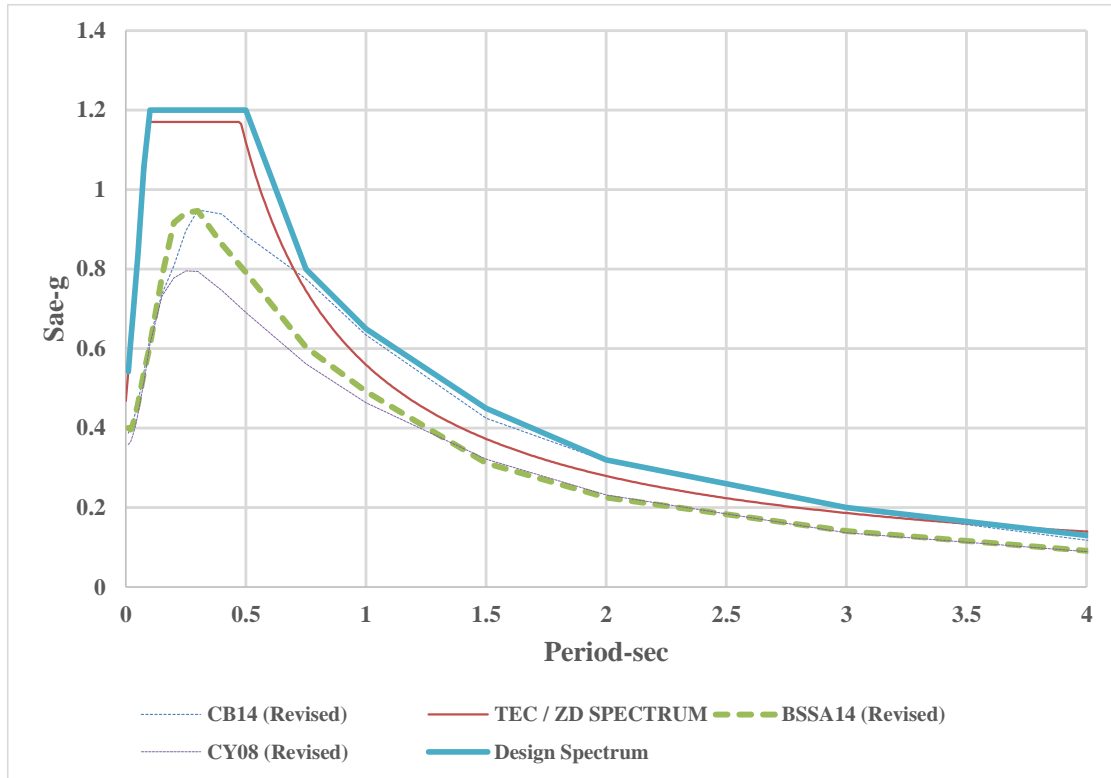
372 Evidence of this behavior was identified during the 2020 Samos Earthquake, especially at Station 3519
373 (Mavişehir–Karşıyaka). A spectral comparison between horizontal components revealed that the N–S component,
374 aligned with the rupture direction, recorded spectral accelerations 1.6 to 2.1 times greater than the transverse (E–
375 W) component within the 1.0–2.0 second period range. This is consistent with studies by Shahi and Baker (2011),
376 Chang et al. (2018), and Bayless et al. (2024), which quantify rupture directivity-induced amplification in near-
377 fault conditions, particularly in the long-period spectral domain relevant to mid- and high-rise buildings.

378 In light of these observations, rupture directivity effects were explicitly accounted for in the development of the
379 target response spectrum. The selected spectrum was constructed to envelope the median predictions from the
380 best-fitting GMPEs as well as the regulatory baseline defined by the Turkish Earthquake Code (TEC-2018).
381 Special emphasis was placed on the 1.0–2.0 second period range, where directivity-induced amplification is most
382 critical. The final deterministic design spectrum (Figure 10) thus integrates:

- 383 • regional seismic source characteristics,
- 384 • site-specific nonlinear amplification behavior,
- 385 • and empirical observations from near-fault recordings.

386

387 This spectrum serves as a robust basis for the performance-based evaluation of future seismic demand across
388 İzmir’s urban basin and provides a realistic representation of shaking intensity under near-fault ground motion
389 conditions.



390

391 **Figure 10.** Proposed target response spectrum for the deterministic Mw 6.5 scenario, incorporating GMPE
392 predictions, TEC-2018 provisions, and directivity-adjusted long-period amplification.

393 4.1. Ground Motion Selection and Spectral Matching

394 A total of 11 ground motion records were selected for the deterministic Mw 6.5 scenario (Table 6) and spectrally
395 matched to the target response spectrum using SeismoMatch (Seismosoft, 2022). All ground-motion records listed
396 in Table 6 were obtained from the PEER NGA-West2 Ground Motion Database. The matching was performed
397 within the 0.1–2.0 s period range, which corresponds to the dominant periods of mid- to high-rise buildings in
398 İzmir. The spectral matching algorithm preserved the nonstationary features and energy content of the original
399 time histories while modifying their frequency content to achieve compatibility with the design spectrum.

400

401

402

403

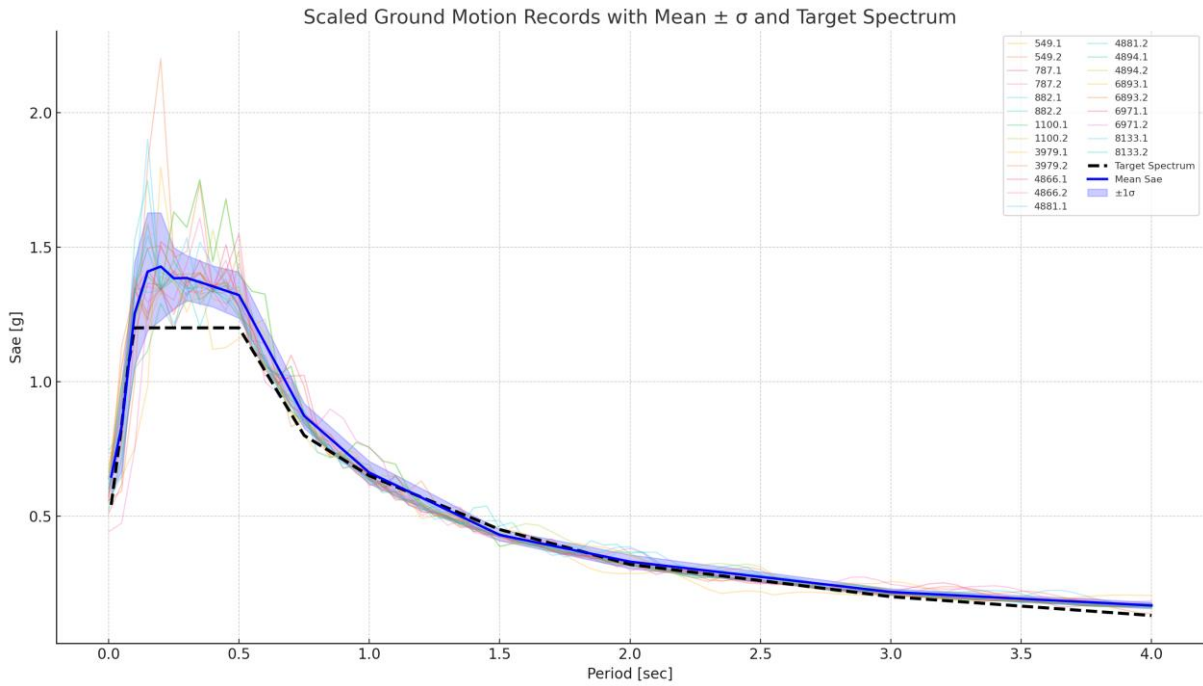
404

No	Record Sequence Number	Scale Factor	Earthquake Name	Year	Station Name	Magnitude	Mechanism	R_jb(km)	R_rup (km)	Vs30 (m/sec)
1	4881	2.32	Chuetsu-oki_Japan	2007	Nagaoka Kouiti Town	6.8	Reverse	11.61	20.77	294.38
2	549	1.91	Chalfant Valley-02	1986	Bishop-LADWP south St.	6.19	Strike Slip	14.38	17.17	303.47
3	6893	1.07	Darfield_New Zealand	2010	DFHS	7	Strike Slip	11.86	11.86	344.02
4	8133	4.31	Christchurch_New Zealand	2011	SLRC	6.2	Reverse Oblique	31.81	31.81	249.28
5	6971	2.12	Darfield_New Zealand	2010	SPFS	7	Strike Slip	29.86	29.86	389.54
6	882	2.57	Landers	1992	Desert Hot Springs	7.28	Strike Slip	26.84	26.84	344.67
7	4866	1.26	Chuetsu-oki_Japan	2007	Kawanishi Izumozaki	6.8	Reverse	0	11.75	338.32
8	4894	0.38	Chuetsu-oki_Japan	2007	Kashiwazaki NPP_Unit 1	6.8	Reverse	0	10.97	329
9	787	1.43	Loma Prieta	1989	Palo Alto - SLAC Lab	6.93	Reverse Oblique	30.62	30.86	425.3
10	1100	2.03	Kobe_Japan	1995	Abeno	6.9	Strike Slip	24.85	24.85	256
11	3979	2.82	San Simeon_CA	2003	Cambria-Hyw 1 Caltrans Bridge	6.52	Reverse	6.97	7.25	362.42

406

407 As illustrated in Figure 11, the matched spectra closely align with the target response spectrum. The mean spectrum
408 of the selected records remains within $\pm 10\%$ of the target over the defined period range, while the $\pm 1\sigma$ envelope
409 effectively captures the record-to-record variability. This level of conformity satisfies compatibility guidelines
410 recommended by Eurocode 8 and PEER-GMSM protocols, which require the mean response spectrum to remain
411 within $\pm 10\%$ of the target and encourage representation of variability through mean $\pm 1\sigma$ spectral envelopes (CEN,
412 2004; Haselton et al., 2011).

413



414

415 Figure 11. Combined plot showing scaled ground motion records, target spectrum (dashed), and the mean $\pm 1\sigma$
 416 spectral envelope of the records.

417 To further quantify the match quality, statistical metrics were computed at discrete periods. These include the
 418 mean spectral acceleration (Sae), standard deviation (σ), and the exceedance rate, defined as the proportion of
 419 records exceeding the target spectrum at each period. The results are summarized in Table 7.

420 The exceedance rate exceeds 90% for periods $T \leq 0.3$ s, indicating strong coverage in the short-period range. At
 421 longer periods ($T > 1.0$ s), the rate decreases, reflecting both the spectral shape of the selected ground motions and
 422 limitations in the scaling process. Nevertheless, the overall spectral compatibility satisfies performance-based
 423 ground motion selection criteria.

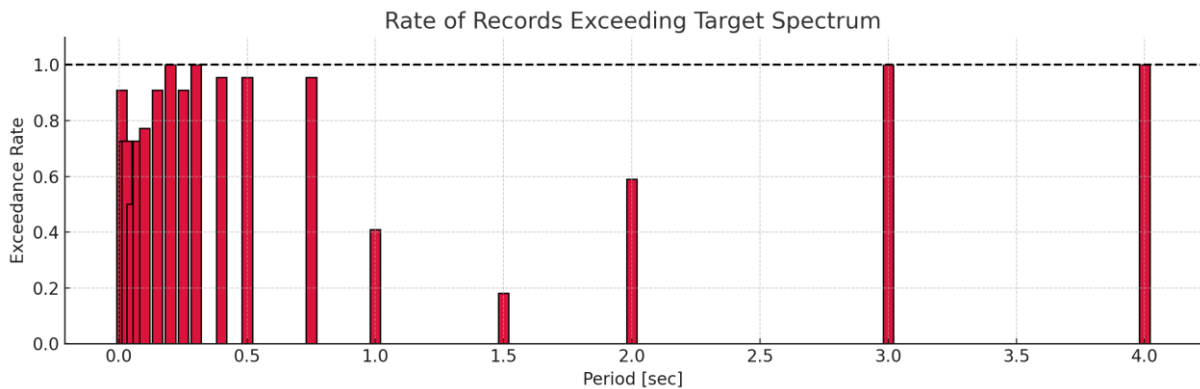
424 **Table 7.** Statistical summary of spectral accelerations (Sae) at selected periods: mean, standard deviation, and exceedance
 425 metrics relative to the target spectrum.

T (sec)	Target Sae (g)	Mean Sae (g)	Std Dev (g)	Exceed Count	Exceedance Rate
0.01	0.54	0.65	0.07	20.00	0.91
0.02	0.62	0.69	0.09	16.00	0.73
0.03	0.69	0.74	0.11	16.00	0.73
0.05	0.84	0.83	0.17	11.00	0.50
0.08	1.06	1.04	0.16	16.00	0.73
0.10	1.20	1.25	0.19	17.00	0.77
0.15	1.20	1.41	0.22	20.00	0.91
0.20	1.20	1.43	0.20	22.00	1.00
0.25	1.20	1.38	0.11	20.00	0.91
0.30	1.20	1.39	0.08	22.00	1.00
0.40	1.20	1.35	0.08	21.00	0.95
0.50	1.20	1.32	0.09	21.00	0.95
0.75	0.80	0.87	0.05	21.00	0.95
1.00	0.65	0.66	0.04	9.00	0.41
1.50	0.45	0.43	0.02	4.00	0.18

2.00	0.32	0.33	0.03	13.00	0.59
3.00	0.20	0.22	0.01	22.00	1.00
4.00	0.13	0.17	0.01	22.00	1.00

426

427 As shown in Figure 12, the exceedance rate distribution confirms strong representation in the short-period range
 428 and reasonable coverage at longer periods, supporting the robustness of the selected ground motion suite for site-
 429 specific nonlinear response analysis.



430

431 Figure 12. Rate of Records Exceeding Target Spectrum

432 In summary, the selected set of spectrally matched ground motions satisfies both code-based compatibility
 433 requirements and statistical representativeness. The resulting record suite provides a robust basis for deterministic
 434 nonlinear site response analysis, accurately capturing spectral variability across the period range of interest and
 435 supporting reliable performance-based seismic design and assessment.

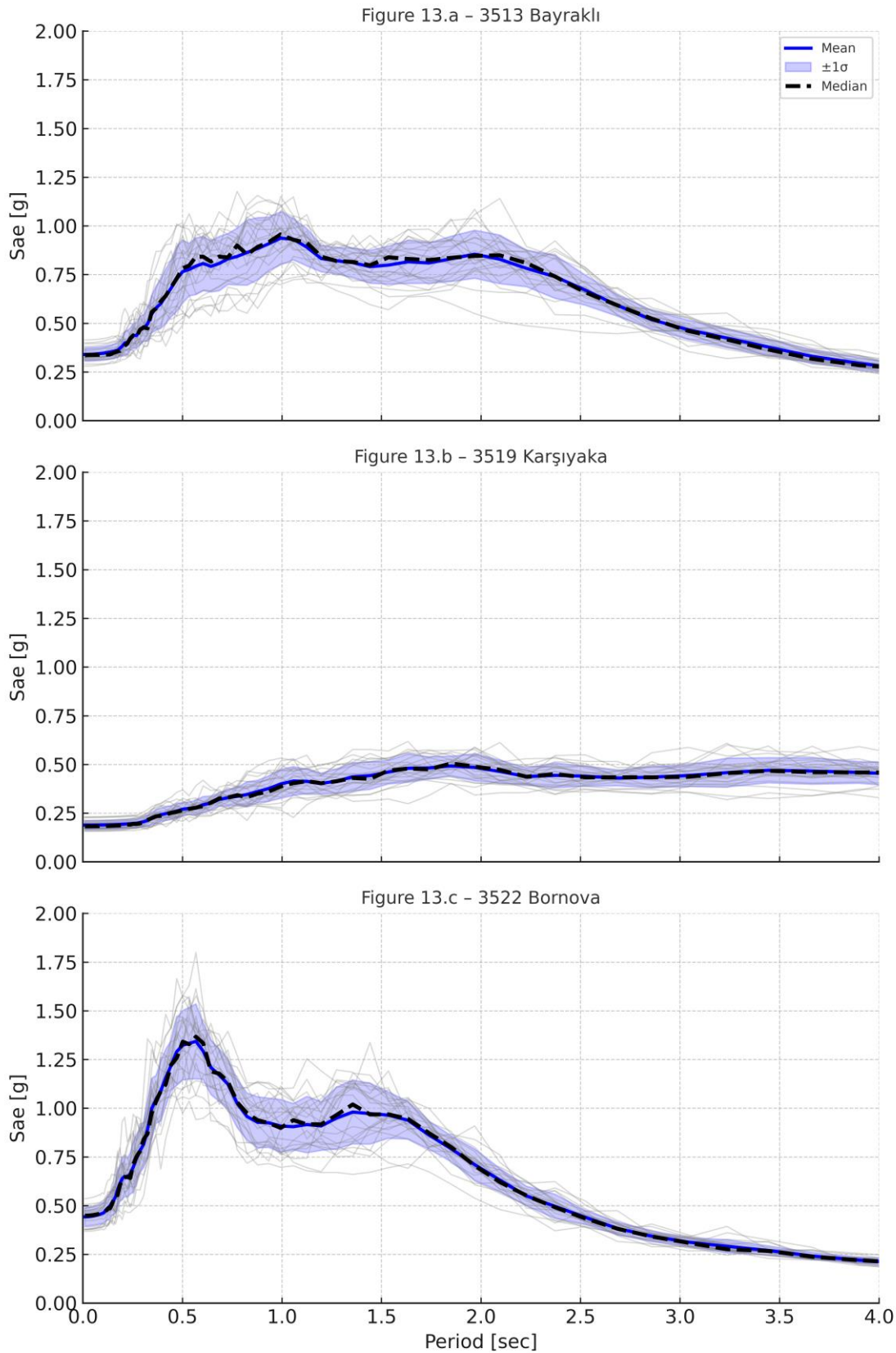
436 4.2. Site-Specific Nonlinear Response Analysis and Comparison with Code-Based Spectra

437 Using the 1D nonlinear site response models calibrated in the previous sections via DEEPSOIL, site-specific
 438 ground response analyses were conducted for each station (3513 – Bayraklı, 3519 – Karşıyaka, and 3522 –
 439 Bornova) under the input of spectrally matched ground motion records. The spectral acceleration outputs at the
 440 surface are presented in Figure 13a-c, including the ensemble of scaled records, the mean $\pm 1\sigma$ variability band,
 441 and the median response spectrum for each site.

442 The results indicate substantial variation in spectral amplification characteristics across stations, driven by
 443 differences in soil stiffness, stratigraphy, and nonlinear soil behavior. The $\pm 1\sigma$ band serves as an envelope of
 444 epistemic uncertainty in record selection, while the median spectrum is used in subsequent engineering demand
 445 parameter (EDP) evaluations as a statistically robust representation of site-specific seismic input, in line with
 446 recommendations from PEER-GMSM Guidelines (Haselton et al., 2011).

447 In Bayraklı and Karşıyaka, which are underlain by deep alluvial deposits, spectral peaks shift toward longer periods
 448 ($T > 1.0$ s), suggesting basin-induced resonance effects (Borcherdt, 1994; Kaklamanos et al., 2013). In contrast,
 449 Bornova exhibits pronounced short-period amplification ($T < 0.5$ s) due to shallower, more compliant layers
 450 overlying stiff substrata.

451 Nonlinear behavior is especially evident in Karşıyaka, where broadened $\pm 1\sigma$ dispersion and flattened median
452 spectra suggest strain-softening, modulus degradation, and hysteretic damping, consistent with behavior described
453 by Hashash et al. (2010) and Vucetic & Dobry (1991).



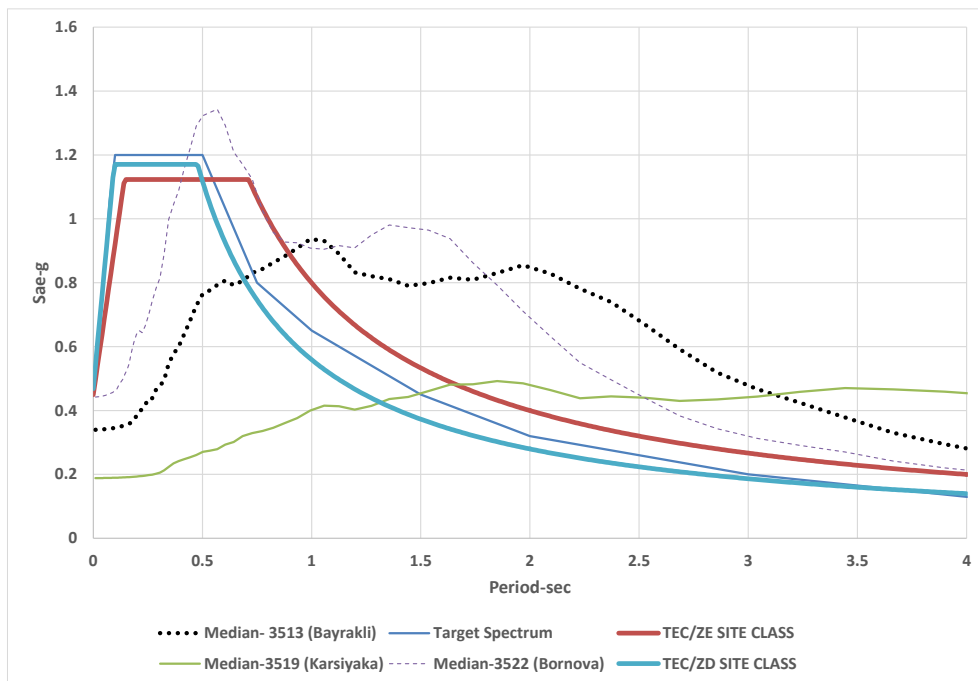
454

455 **Figure 13.** Scaled spectral acceleration (Sae) records for three selected sites: 3513 – Bayraklı, (b) 3519 –
 456 Karşıyaka, and (c) 3522 – Bornova. Each subplot includes the ensemble of scaled motions (gray lines), the mean
 457 spectrum (blue), $\pm 1\sigma$ variability band (shaded), and the median response spectrum (black dashed)

458 Figure 14 compares the median spectra from SRA with the uniform hazard spectrum (UHS) and code-defined
 459 design spectra (TEC, 2018) for Site Classes ZE and ZD. Across all three sites, clear deviations are observed:

- 460 • Bayraklı and Karşıyaka: Peak amplifications occur in $T > 1.0$ s range—significantly exceeding TEC
- 461 curves.
- 462 • Bornova: Amplification is dominant in $T < 0.5$ s range, revealing frequency-dependent site response.

463 These differences demonstrate that code-based spectral shapes do not adequately reflect site-specific effects in
 464 deep alluvial environments.



465 Figure 14. Median spectral acceleration (Sae) curves obtained from scaled ground motions for three different sites
 466 (Bayraklı, Karşıyaka, Bornova), compared with the uniform hazard spectrum (Target Spectrum) and the regulatory
 467 spectra defined in the Turkish Earthquake Code (2018) for Site Classes ZE and ZD.
 468

469 According to TEC, the effect of local soil conditions is incorporated through two modification factors, F_S and F_1 ,
 470 which are used to calculate the design spectral acceleration values as follows:

$$471 S_{ds} = S_S \cdot F_S \text{ and } S_{d1} = S_1 \cdot F_1 \quad (2)$$

472 where:

- 473 • S_{ds} is the design spectral acceleration for short-period structures (typically affecting low-rise buildings),

- 474 • S_{d1} is the design spectral acceleration at a 1.0-second period (affecting mid- to high-rise buildings),
- 475 • S_S and S_1 are the reference spectral accelerations on rock or firm soil (Type A/B),
- 476 • F_S and F_1 are site amplification factors defined in TEC based on soil class (e.g., ZE, ZD).

477 However, results of the site-specific response analyses revealed that the actual site amplification ratios (SAR)
 478 derived from ground motion simulations significantly exceed the TEC-defined values, particularly for F_1 , which
 479 controls long-period demands. These findings are summarized in Table 8, where the ratio of F_1_SAR to F_1_TEC
 480 demonstrates the magnitude of underestimation in current code-based designs.

481 Table 8. Local site modification factors (F_1) according to TEC and SAR of scenario earthquake

Station	V_{s30}	Soil Class (Acc TEC)	F_1/ TEC	$F_1/ SAR, t=1 \text{ sec}$
3513	195	ZD	2.054	4.21
3522	249	ZD	2.054	4.76
3519	131	ZE	2.935	4.40

483 4.3. Engineering Implications for Performance-Based Design

484 This amplification behavior has critical design implications, particularly for reinforced concrete (RC) moment-
 485 resisting frames with 3 to 10 stories, which have fundamental periods in the 0.5–1.5 s range. According to TEC
 486 (2018), such structures are expected to meet:

- 487 • Life Safety (LS) under the Design Earthquake (DD-2), and
- 488 • Collapse Prevention (CP) under the Maximum Considered Earthquake (DD-1).

489 However, in sites like Bornova, the median spectral acceleration at $T = 1.0$ s exceeds the TEC value by a factor of
 490 4.76. This discrepancy may result in:

- 491 • Underestimation of interstory drift demands,
- 492 • Increased likelihood of plastic hinge formation,
- 493 • Potential exceedance of performance limits, even when structures comply with code-based spectra.

494 Therefore, these findings underscore the necessity of refining design input parameters—either by modifying the
 495 amplification factor F_1 or adopting fully site-specific response spectra—to ensure accurate seismic demand
 496 estimation and adequate structural performance on deep soft soils.

497 This conclusion aligns with international research (e.g., Stewart & Seyhan, 2013; Pitilakis et al., 2013), which has
 498 shown that empirical site-class-based amplification factors often underestimate long-period spectral demands,
 499 particularly in sedimentary basins with complex stratigraphy and low shear-wave velocities.

500

501

502

503 5. Summary and Conclusions

504 5.1. Summary of the methodology

505 This study aimed to assess site-specific seismic demands for the city of İzmir by integrating empirical ground
506 motion data, GMPE evaluation, and 1D nonlinear site response analyses. The major components of the
507 methodology and key findings are summarized as follows:

- 508 • Firstly, using a dataset of past recorded earthquake events, the level of agreement with current GMPE
509 equations was investigated. Based on the residual analysis, two GMPEs were selected that showed the
510 best consistency with the observed recordings in İzmir, and were subsequently used for defining target
511 spectrum parameters in the site-specific seismicity analysis. Despite being NGA-West2 models, these
512 GMPEs exhibited systematic residuals reaching up to ± 0.3 log units, indicating the necessity for
513 regionally calibrated models for İzmir.
- 514 • To perform site-specific seismic analyses, well-recorded event of İzmir-Samos earthquake data were
515 utilized. A 1D analysis model, using the available geotechnical data was applied for 3 different stations.
516 These stations were selected for the aim to
 - 517 ○ represent different alluvial soil conditions of the city
 - 518 ○ take in to account of the 3 most populated, therefore representative regions of the city
 - 519 ○ be able to arrive a more general conclusion about the possible future earthquake simulations
- 520 • A future deterministic scenario earthquake with $M_w = 6.5$ was developed for the İzmir Fault, following
521 the RADIUS (2005) framework and supported by recent tectonic models. The resulting target spectrum
522 was enhanced by incorporating near-field and directivity effects, resulting in significant modifications to
523 spectral shape and amplitude—particularly at intermediate and long periods. The modified target
524 spectrum exhibits 65–80% higher amplitudes compared to the TEC (2018) code spectra for ZE and ZD
525 classes over the $T = 0.3$ – 1.0 s range. To maintain regulatory consistency, the TEC (2018) was also used
526 to define the baseline hazard level corresponding to a 475-year return period (i.e., 10% probability of
527 exceedance in 50 years).
- 528 • Eleven recorded strong ground motions were selected and spectrally matched to the scenario-specific
529 target spectrum using SeismoMatch. These matched records were used as input for 1D nonlinear
530 simulations at the three selected sites, enabling deterministic estimation of surface-level spectral
531 accelerations under future earthquake conditions.

532 5.2. Key Findings

533 The key findings of this study are as follows:

- 534 • **Validation with the 2020 Samos Earthquake:** The 2020 Samos earthquake has been a significant event
535 for site-specific seismicity studies due to the abundance of recording stations and the rich data content
536 available. Analyses based on this event showed distinct spectral amplifications, particularly in the long-
537 period range ($T > 1.0$ s), which is critical for mid- and high-rise building design.
- 538 • **GMPE Evaluation and Region-Specific Spectral Characterization:** Residual-based comparisons of
539 GMPEs enabled the selection of the most appropriate models for İzmir. Despite their global robustness,

540 the selected NGA-West2 models exhibited systematic residuals up to ± 0.3 log units, emphasizing the
541 need for regionally calibrated ground motion models that better reflect İzmir's unique tectonic and
542 geotechnical conditions.

543 • **Effect of Directivity and Near-Fault Conditions on the Target Spectrum:** By incorporating rupture
544 directivity and near-field effects, the target spectrum was significantly enhanced, particularly within the
545 0.5–1.5 s period range. Compared to the standard code-based spectra (TEC, 2018), the resulting spectrum
546 showed 65–80% higher spectral accelerations, underscoring the importance of including these effects in
547 future national code revisions.

548 • **Observed Site Amplification and Implications for Design Parameters:** Site-specific simulations
549 revealed that surface spectral acceleration at $T = 1.0$ s was amplified by factors of 2.5 to 4.8, depending
550 on location. The median response spectra yielded the following amplification ratios when compared to
551 TEC-based F_1 values:

- 552 ○ Bornova: $S_a = 0.91$ g vs. $TEC = 0.19$ g $\rightarrow F_1$ ratio = 4.76
- 553 ○ Bayraklı: $S_a = 0.73$ g vs. $TEC = 0.19$ g $\rightarrow F_1$ ratio = 3.84
- 554 ○ Karşıyaka: $S_a = 0.56$ g vs. $TEC = 0.19$ g $\rightarrow F_1$ ratio = 2.93

555 These findings clearly indicate that the site amplification factors (F_1) in the Turkish Earthquake Code
556 significantly underestimate long-period demand, particularly in deep alluvial basins.

557 • **Design Relevance for Critical Building Classes:** The underestimation is especially critical for 3–10
558 story reinforced concrete moment-resisting frame structures, whose natural periods ($T = 0.5$ – 1.5 s) fall
559 within the affected range. These buildings are typically designed to meet Life Safety (LS) under the
560 Design Earthquake (DD-2) and Collapse Prevention (CP) under the Maximum Considered Earthquake
561 (DD-1) per TEC (2018). Failure to account for local amplification may lead to:

- 562 ○ Underestimation of interstory drift,
- 563 ○ Inadequate detailing for plastic hinge zones,
- 564 ○ Potential exceedance of performance thresholds.

565 • **Representativeness of Site Selection and Implications for Basin-Wide Analysis:** The selection of
566 three sites (Bayraklı, Karşıyaka, Bornova) provided a basis for understanding the variability of seismic
567 response across İzmir. This approach lays the groundwork for future studies exploring basin effects,
568 nonlinear soil behavior, and wave propagation phenomena in more complex 2D/3D models.

569 • **Need for Region-Specific Seismic Design Frameworks:** The residual trends observed in the GMPE
570 evaluations—despite using globally recognized models—reinforce the need for site-specific and
571 regionally adjusted ground motion models in seismic hazard mitigation. These findings support a growing
572 consensus in the literature that generic site classification frameworks are insufficient in deep sedimentary
573 basins with significant impedance contrasts and complex source mechanisms.

574 **5.3. Limitations and Recommendations for Future Work**

575 While the present study provides valuable insights into local site amplification and spectrum compatibility in İzmir,
576 several limitations should be acknowledged to guide future research:

577 First, the site response analyses were conducted using 1D equivalent-linear models, calibrated with available
578 geotechnical and seismic data. Although these models are widely accepted for practical applications, they do not
579 fully capture three-dimensional basin effects, such as lateral wave propagation, edge-generated surface waves, and
580 spatial variability in soil layering and shear-wave velocity. Incorporating 2D or 3D nonlinear models would
581 improve the accuracy of response predictions, especially in complex alluvial basins like İzmir.

582 Second, the study adopted a deterministic $M_w = 6.5$ earthquake scenario, based on the İzmir Fault. While this
583 provides valuable insight into scenario-based seismic demands, it limits the exploration of multi-source
584 interactions and epistemic uncertainties inherent in probabilistic seismic hazard assessments (PSHA). Future work
585 should integrate probabilistic frameworks to account for the full range of potential seismic sources, magnitudes,
586 and recurrence rates.

587 Third, the spectrally matched ground motions were scaled to a single intensity level (e.g., 475-year return period).
588 While this is consistent with design-level evaluation, it may not adequately address varying intensity measure
589 levels (IMLs) required for performance-based seismic design (PBD) or fragility analysis. Future studies should
590 incorporate multi-level hazard scenarios to capture demand variability and damage probability more
591 comprehensively.

592 To address these limitations and advance the regional seismic assessment framework, future research could
593 explore:

- 594 • Fully nonlinear time-domain simulations, accounting for strain-dependent soil behavior and cyclic
595 degradation,
- 596 • 3D geotechnical modeling, especially for large-scale basin structures and lateral heterogeneity,
- 597 • Machine-learning-based surrogate modeling, to improve computational efficiency and enable real-time
598 seismic risk screening across urban areas.

599 Although this study is rooted in the geotechnical and tectonic conditions of İzmir, the developed methodology
600 offers a generalizable and transferable framework for other seismically active urban areas underlain by deep
601 alluvial or sedimentary basins. By integrating residual-based GMPE selection, site-specific spectrum development,
602 and nonlinear site response analysis, this study bridges the gap between code-level design assumptions and
603 localized seismic demand.

604 Ultimately, the findings contribute to the development of a more resilient seismic design paradigm, emphasizing
605 the critical role of site-specific response analysis in modern performance-based engineering, particularly for
606 infrastructure located in complex geologies where empirical code factors may not suffice.

607 **Funding** The authors declare that no funds, grants, or other support were received during the preparation of his
608 manuscript.

609 **Data availability** all data and models analyzed during the current study are available from the corresponding
610 author on reasonable request.

611 **Declarations**

612 **Competing interests** the authors have no relevant financial or non-financial interests to disclosure.

613 **Acknowledgements** The authors gratefully acknowledge AFAD for providing the strong-motion recordings of the
614 2020 Samos Earthquake, and the Pacific Earthquake Engineering Research Center (PEER) for maintaining and
615 providing access to the NGA-West2 ground-motion database. The continuous efforts of the contributing
616 observation networks and institutions are sincerely appreciated

617 **6. References**

- 618 Abrahamson NA, Silva W. Summary of the Abrahamson & Silva NGA groundmotion relations. *Earthq Spectra* 2008;24:67–
619 97. <https://doi.org/10.1193/1.2924360>
- 620 Abrahamson NA, Silva WJ, Kamai R. Summary of the ASK14 ground motion relation for active crustal regions. *Earthq Spectra*
621 2014;30:1025–55. <https://doi.org/10.1193/070913EQS198M>
- 622 Akyol, N., Zhu, L., Mitchell, B. J., Sözbilir, H., & Kekovalı, K. (2006). Crustal structure and local seismicity in western
623 Anatolia. *Geophysical Journal International*, 166(3), 1259–1269. <https://doi.org/10.1111/j.1365-246X.2006.03053.x>
- 624 Akkar, S., & Bommer, J. J. (2010). Empirical equations for the prediction of PGA, PGV, and spectral accelerations in Europe,
625 the Mediterranean region, and the Middle East. *Seismological Research Letters*, 81(2), 195–206.
626 <https://doi.org/10.1785/gssrl.81.2.195>
- 627 Akkar, S., Sandıkkaya, M. A., & Bommer, J. J. (2014). Empirical ground-motion models for point- and extended-source crustal
628 earthquake scenarios in Europe and the Middle East. *Bulletin of Earthquake Engineering*, 12(1), 359–387.
629 <https://doi.org/10.1007/s10518-013-9461-4>
- 630 Basili, R., Danciu, L., Beauval, C., Sesetyan, K., Vilanova, S. P., Adamia, S., Arroucau, P., Atanackov, J., Baize, S., Canora,
631 C., Caputo, R., Carafa, M. M. C., Cushing, E. M., Custódio, S., Demircioglu Tumsa, M. B., Duarte, J. C., Ganas, A., García-
632 Mayordomo, J., Gómez De La Peña, L., ... Giardini, D. (2024). The European Fault-Source Model 2020 (EFSM20): geologic
633 input data for the European Seismic Hazard Model 2020. *Natural Hazards and Earth System Sciences*, 24(11).
634 <https://doi.org/10.5194/nhess-24-3945-2024>
- 635 Bayless, J., Abrahamson, N. A., & Somerville, P. (2024). A rupture directivity adjustment model and its application in seismic
636 hazard analysis. *Earthquake Spectra*.
- 637 Boore DM, Atkinson GM (2008) Ground-motion prediction equations for the average horizontal component of PGA, PGV,
638 and 5%-damped PSA at spectral periods between 0.01 s and 10.0 s. *Earthq Spectra* 24:99–138.
639 <https://doi.org/10.1193/1.2830434>
- 640 Boore DM, Stewart JP, Seyhan E, Atkinson GM. NGA-West2 equations for predicting PGA, PGV, and 5% damped PSA for
641 shallow crustal earthquakes. *Earthq Spectra* 2014;30:1057–85. <https://doi.org/10.1193/070113EQS184M>
- 642 Borchardt, R. D. (1994). Estimates of site-dependent response spectra for design (methodology and justification). *Earthquake*
643 *Spectra*, 10(4), 617–653. <https://doi.org/10.1193/1.1585791>
- 644 Campbell KW, Bozorgnia Y. NGA ground motion model for the geometric mean horizontal component of PGA, PGV, PGD
645 and 5% damped linear elastic response spectra for periods ranging from 0.01 to 10 s. *Earthq Spectra* 2008;24:139–71.
646 <https://doi.org/10.1193/1.2857546>
- 647 Campbell KW, Bozorgnia Y. NGA-West2 ground motion model for the average horizontal components of PGA, PGV, and 5%
648 damped linear acceleration response spectra. *Earthq Spectra* 2014;30:1087–115. <https://doi.org/10.1193/062913EQS175M>.
- 649 CEN. (2004). Eurocode 8: Design of structures for earthquake resistance – Part 1: General rules, seismic actions and rules for
650 buildings (EN 1998-1:2004). Brussels: European Committee for Standardization.
- 651 Cetin, K. Ö., Altun, S., Askan, A., Akgün, M., Sezer, A., Kınca, C., ... & Karaali, E. (2022). The site effects in Izmir Bay of
652 October 30, 2020, M7.0 Samos Earthquake. *Soil Dynamics and Earthquake Engineering*, 152, 107051.
653 <https://doi.org/10.1016/j.soildyn.2021.107051>

- 654 Cetin, K. Ö., Zazour, M., Çakır, E., Tuna, S. Ç., & Altun, S. (2023). 2-D and 3-D basin site effects in Izmir–Bayrakli during
655 the October 30, 2020 Mw7.0 Samos earthquake. *Bulletin of Earthquake Engineering*, 21, 5419–5442.
656 <https://doi.org/10.1007/s10518-023-01738-3>
- 657 Cetin, K.O., Cakir, E. & Zazour, M. Seismic site effect models for the Turkiye-Izmir-Bayrakli Basin. *Bull Earthquake Eng*
658 22, 303–328 (2024). <https://doi.org/10.1007/s10518-023-01774-z>
- 659 Chang, Z., Sun, X., Zhai, C., Zhao, J. X., & Xie, L. (2018). An empirical approach of accounting for the amplification effects
660 induced by near fault directivity. *Bulletin of Earthquake Engineering*, 16(5), 1871–1885.
- 661 Chiou, B.S.J. and Youngs, R.R. (2008) An NGA Model for the Average Horizontal Component of Peak Ground Motion and
662 Response Spectra. *Earthquake Spectra*, 24, 173-215. <https://doi.org/10.1193/1.2894832>
- 663 Chiou BSJ, Youngs RR. Update of the Chiou and Youngs NGA model for the average horizontal component of peak ground
664 motion and response spectra. *Earthq Spectra* 2014;30:1117–53. <https://doi.org/10.1193/072813EQS219M>
- 665 Dan McKenzie, Active tectonics of the Alpine—Himalayan belt: the Aegean Sea and surrounding regions, *Geophysical Journal*
666 *International*, Volume 55, Issue 1, October 1978, Pages 217–254, <https://doi.org/10.1111/j.1365-246X.1978.tb04759.x>
- 667 Danciu, L., Giardini, D., Weatherill, G., Basili, R., Nandan, S., Rovida, A., Beauval, C., Bard, P.-Y., Pagani, M., Reyes, C. G.,
668 Sesetyan, K., Vilanova, S., Cotton, F., and Wiemer, S.: The 2020 European Seismic Hazard Model: overview and results, *Nat.*
669 *Hazards Earth Syst. Sci.*, 24, 3049–3073, <https://doi.org/10.5194/nhess-24-3049-2024>, 2024.
- 670 Emre, Ö., Duman, T.Y., Özalp, S. et al. Active fault database of Turkey. *Bull Earthquake Eng* 16, 3229–3275 (2018).
671 <https://doi.org/10.1007/s10518-016-0041-2>
- 672 Emre O, Ozalp S, Dogan A, Ozaksoy V, Yildirim C, Goktas F (2005) Active faults in the vicinity of Izmir and their earthquake
673 potentials [in Turkish], Report No: 10754, Geological Studies Department, General Directorate of Mineral Research and
674 Exploration, Ankara, Turkey
- 675 FEMA (2001). NEHRP recommended provisions for seismic regulations for new buildings and other structures (FEMA 368).
676 Washington, DC: Federal Emergency Management Agency.
- 677 Gülerce, Z., Akbaş, B., Özacar, A. A., Sopacı, E., Önder, F. M., & Bora, S. S. (2022). Predictive performance of current ground
678 motion models for recorded strong motions in 2020 Samos Earthquake. *Soil Dynamics and Earthquake Engineering*, 152,
679 107053. <https://doi.org/10.1016/j.soildyn.2021.107053>
- 680 Haselton, C. B., Baker, J. W., Liel, A. B., Deierlein, G. G., Bozorgnia, Y., & Curtin, P. (2011). Evaluation of ground motion
681 selection and modification methods: Predicting median interstory drift response of buildings (PEER Report No. 2011/03).
682 Pacific Earthquake Engineering Research Center, University of California, Berkeley.
- 683 Hashash, Y. M. A., Park, D., & Phillips, C. A. (2010). Evaluation of ground motion analysis procedures for seismic design of
684 deep foundations. PEER Report 2010/05, University of California, Berkeley.
- 685 Hashash YMA, Musgrove MI, Harmon JA, Ilhan O, Xing G, Numanoglu O. DEEPSOIL V7.0, User manual. Urbana, IL: Board
686 of Trustees of University of Illinois at Urbana-Champaign; 2020
- 687 Kaklamanos, J., Baise, L. G., Boore, D. M., & Thompson, E. M. (2013). Implementation of a VS30-based nonlinear site
688 amplification model for NEHRP site classes C and D in the NGA-West2 database. *Bulletin of the Seismological Society of*
689 *America*, 103(1), 211–228. <https://doi.org/10.1785/0120120195>
- 690 Kalkan, E., & Gülkan, P. (2004). Site-dependent spectra derived from ground-motion records Turkey. *Earthquake Spectra*,
691 20(4), 1111–1138. <https://doi.org/10.1193/1.1810233>
- 692 Kramer SL (1996) *Geotechnical earthquake engineering*, Prentice Hall, Upper Saddle River
- 693 Kwok, A. O. L., Stewart, J. P., Hashash, Y. M. A., Matasovic, N., Pyke, R., Wang, Z., & Yang, Z. (2007). Use of Exact
694 Solutions of Wave Propagation Problems to Guide Implementation of Nonlinear Seismic Ground Response Analysis
695 Procedures. *Journal of Geotechnical and Geoenvironmental Engineering*, 133(11). [https://doi.org/10.1061/\(asce\)1090-0241\(2007\)133:11\(1385\)](https://doi.org/10.1061/(asce)1090-0241(2007)133:11(1385))
- 696
- 697 Ocañoğlu, F., Demirbağ, E., & Kuşçu, İ. (2005). Neotectonic structures in İzmir Gulf and surrounding regions (western
698 Turkey): Evidences of strike-slip faulting with compression in the Aegean extensional regime. *Marine Geology*, 219(2–3),
699 155–171. <https://doi.org/10.1016/j.margeo.2005.06.004>
- 700 Pitilakis, K., Riga, E., & Anastasiadis, A. (2013). New code site classification, amplification factors and normalized response
701 spectra based on a worldwide ground-motion database. *Bulletin of Earthquake Engineering*, 11(4).
702 <https://doi.org/10.1007/s10518-013-9429-4>

703 RADIUS (1997), Risk assessment tools for diagnosis of urban areas against seismic disaster Izmir earthquake master program,
704 Bogazici University Kandilli Observatory, Istanbul, Turkey

705 Seed, H. B., and Idriss, I. M. (1970). "Soil moduli and damping factors for dynamic response analyses," Report No. EERC 70-
706 10, Earthquake Engineering Research Center, Univ. of California, Berkeley, California. Berkeley, December.

707 Seismosoft. (2022). SeismoMatch v2022 – Spectrum matching software. <https://seismosoft.com>

708 Shahi, S. K., & Baker, J. W. (2011). An empirically calibrated framework for including the effects of near-fault directivity in
709 probabilistic seismic hazard analysis. *Bulletin of the Seismological Society of America*, 101(2), 742–755.

710 Somerville, P. G., Smith, N. F., Graves, R. W., & Abrahamson, N. A. (1997). Modification of empirical strong ground motion
711 attenuation relations to include the amplitude and duration effects of rupture directivity. *Seismological Research Letters*, 68(1),
712 199–222. <https://doi.org/10.1785/gssrl.68.1.199>

713 Stewart, J. P., & Seyhan, E. (2013). Semi-empirical nonlinear site amplification and its application in NEHRP site factors. In
714 Berkeley, United States of America: Pacific Earthquake Engineering Research Center (Issue November).

715 Tepe, Ç., Sözbilir, H., Eski, S., Sümer, Ö., & Özkaymak, Ç. (2021). Updated historical earthquake catalog of İzmir region
716 (western Anatolia) and its importance for the determination of seismogenic source. *Turkish Journal of Earth Sciences*, 30(8),
717 Article 6. <https://doi.org/10.3906/yer-2101-14>

718 Tsai, C.-C., & Li, P.-C. (2024). Quantifying near-fault motion effects on soil liquefaction through effective stress site response
719 analysis. *Soil Dynamics and Earthquake Engineering*, 183, 108779. <https://doi.org/10.1016/j.soildyn.2024.108779>

720 Tsai, C.-C., & Liu, H.-W. (2017). Site response analysis of vertical ground motion in consideration of soil nonlinearity. *Soil*
721 *Dynamics and Earthquake Engineering*, 102, 124–136. <https://doi.org/10.1016/j.soildyn.2017.08.024>

722 Ministry of Environment and Urbanization. (2018). Turkish Building Earthquake Code (TEC 2018). Ankara, Turkey: Republic
723 of Turkey, Ministry of Environment and Urbanization.

724 Turkish Ministry of Interior Disaster and Emergency Management Presidency (AFAD), Ankara, Türkiye,
725 <https://tadas.afad.gov.tr>

726 Vucetic, M. and Dobry, R. (1991) Effect of Soil Plasticity on Cyclic Response. *Journal of Geotechnical Engineering*, 117, 89-
727 107. [http://dx.doi.org/10.1061/\(ASCE\)0733-9410\(1991\)117:1\(89\)](http://dx.doi.org/10.1061/(ASCE)0733-9410(1991)117:1(89))

728 Zalachoris, G., & Rathje, E. M. (2015). Evaluation of one-dimensional site response techniques using borehole arrays. *Journal*
729 *of Geotechnical and Geoenvironmental Engineering*, 141(8), 04015053. [https://doi.org/10.1061/\(ASCE\)GT.1943-5606.0001366](https://doi.org/10.1061/(ASCE)GT.1943-5606.0001366)
730